Critical Level Crossings and Gapless Spin Liquid in the Square-Lattice Spin-1/2 J_{1}-J_{2} Heisenberg Antiferromagnet

Ling Wang and Anders W. Sandvik

Phys. Rev. Lett. **121**, 107202 — Published 4 September 2018

DOI: 10.1103/PhysRevLett.121.107202

Critical level crossings and gapless spin liquid in the square-lattice spin-1/2 J_1-J_2 Heisenberg antiferromagnet

Ling Wang[1,*] and Anders W. Sandvik[2,1,3,†]

[1] *Beijing Computational Science Research Center, 10 East Xibeiwang Rd, Beijing 100193, China*
[2] *Department of Physics, Boston University, 590 Commonwealth Ave, Boston, Massachusetts 02215, USA*
[3] *Beijing National Laboratory of Condensed Matter Physics and Institute of Physics, Chinese Academy of Sciences, Beijing 100190, China*

(Dated: August 7, 2018)

We use the DMRG method to calculate several energy eigenvalues of the frustrated $S = 1/2$ square-lattice J_1-J_2 Heisenberg model on $2L \times L$ cylinders with $L \leq 10$. We identify excited-level crossings versus the coupling ratio $g = J_2/J_1$ and study their drifts with the system size L. The lowest singlet-triplet and singlet-quintuplet crossings converge rapidly (with corrections $\propto L^{-2}$) to different g values, and we argue that these correspond to ground-state transitions between the Néel antiferromagnet and a gapless spin liquid, at $g_{c1} \approx 0.46$, and between the spin liquid and a valence-bond-solid at $g_{c2} \approx 0.52$. Previous studies of order parameters were not able to positively discriminate between an extended spin liquid phase and a critical point. We expect level-crossing analysis to be a generically powerful tool in DMRG studies of quantum phase transitions.

The spin-1/2 frustrated J_1-J_2 Heisenberg model on the two-dimensional (2D) square lattice (where J_1 and J_2 are the strengths of the first and second neighbor couplings $\mathbf{S}_i \cdot \mathbf{S}_j$, respectively) has been studied and debated since the early days of the high-T_c cuprate superconductors [1–12]. The initial interest in the system stemmed from the proposal that frustrated antiferromagnetic (AFM) couplings could lead to a spin liquid (SL) in which preformed pairs (resonating valence bonds [13]) become superconducting upon doping [14, 15]. Later, with frustrated quantum magnets emerging in their own right as an active research field [16], the J_1-J_2 model became a prototypical 2D system for theoretical and computational studies of quantum phase transitions and nonmagnetic states [17–33]. Of primary interest is the transition from the long-range Néel AFM ground state [34–36] at small $g = J_2/J_1$ to a nonmagnetic state in a window around $g \approx 0.5$ (before a stripe AFM phase at $g \gtrsim 0.6$). The nature of this quantum phase transition has remained enigmatic [12, 17–21], despite a large number of calculations with numerical tools of ever increasing sophistication, e.g., the density matrix renormalization group (DMRG) method [28, 29, 37, 38], tensor-product states [20, 21, 30–33], and variational Monte Carlo [27, 39].

The nonmagnetic state may be one with spontaneously broken lattice symmetries due to formation of a pattern of singlets (a valence-bond-solid, VBS) or a SL. Within these two classes of potential ground states there are several different proposals, e.g., a columnar [6, 7, 12] versus a plaquette [17, 23, 29, 31] VBS, and gapless [27] or gapped [28] SLs. The quantum phase transition out of the AFM state may possibly be an unconventional 'deconfined' transition [40–42], which recently has been investigated primarily within other models [43–51] hosting direct AFM–VBS transitions. In the J_1-J_2 model, some studies have indicated that the nonmagnetic phase may actually comprise two different phases, with an entire gapless SL phase—not just a critical point—existing between the AFM and VBS states [29, 39]. However, because of the small system sizes accessible, it was not possible to rule out a direct AFM–VBS transitions. We here demonstrate an intervening gapless SL by locating the AFM–SL and SL-VBS transitions using a numerical level-spectroscopy approach, where finite-size transition points are defined using excited-level crossings. These crossing points exhibit smooth size dependence and can be more reliably extrapolated to infinite size than the order parameters and gaps used in past studies.

We use a variant of the DMRG method [37, 38, 52, 53] to calculate the ground state energy as well as several of the lowest singlet, triplet and quintuplet excited energies. In the AFM state, the lowest excitation above the singlet ground state in a finite system with an even number of sites is a triplet—the lowest state in the Anderson tower of 'quantum rotor' states [34]. If the nonmagnetic ground state is a degenerate singlet when the system length $L \to \infty$, as it should be in both a VBS and a topological (gapped) SL, there must be a crossing of the lowest singlet and triplet excitation at a point $g(L)$ that approaches g_c with increasing L. This is indeed observed at the dimerization transition of the 1D J_1-J_2 chain [54–56] and related systems [57, 58], and size extrapolations give g_c to remarkable precision, even with system sizes only up to $L \approx 30$. A level crossing with the same finite-size behavior was observed recently also in the 2D J-Q model [59], which is a Heisenberg model supplemented by four-spin interactions causing an AFM–VBS transition [43–49], likely a deconfined quantum-critical point with unusual scaling properties [50]. It is then natural to investigate level crossings also in the 2D J_1-J_2 model.

We will demonstrate a singlet-triplet level crossing in the J_1-J_2 model which for $2L \times L$ cylindrical lattices shifts as $g_{c2} - g_{c2}(L) \propto L^{-2}$ and converges to $g_{c2} \approx 0.52$. We also observe a singlet-quintuplet level crossing, which

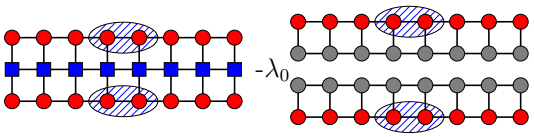

FIG. 1. Illustration of the effective Hamiltonian $H^1_{\rm eff}$ below in Eq. (1). Red and gray circles represent the targeted state $|\psi_1\rangle$ and the ground state $|\psi_0\rangle$, respectively, and the blue squares show the original Hamiltonian as a matrix-product operator. The hatched area represents $U_1^\dagger|\psi_1\rangle$, where U_1 projects to the canonical MPS for $|\psi_1\rangle$ without the hatched area.

converges to a different point, $g_{c1} \approx 0.46$. Given the known transitions associated with singlet-triplet crossings, and that a singlet-quintuplet crossing was found at the transition between the critical and AFM states in a Heisenberg chain with long-range interactions [56, 60], we interpret both g_{c1} and g_{c2} as quantum-critical points. For $g_{c1} \leq g \leq g_{c2}$ the system appears to be a gapless SL with algebraically decaying correlations, as in one of the scenarios proposed in Refs. 29 and 39 (and previously discussed also in Ref. 61). Our value of g_{c1} is in the middle of the range $g = 0.4 \sim 0.5$ where most recent studies have put the end of the AFM phase [27–29, 39], and g_{c2} is close to the VBS-ordering point in Refs. 29 and 39.

DMRG calculations.—The DMRG method [37] is a powerful tool for computing the ground state $|\psi_0\rangle$ of a many-body Hamiltonian. By solving a Hamiltonian $H_{\rm eff}$ in a relevant low-entangled subspace of the full Hilbert space, one can obtain an effective wavefunction, through which the most relevant subspace is selected for the next iteration. A series of such subspace projectors produces the ground state as a matrix product state (MPS), i.e., the wavefunction coefficients are traces of products of local matrices of chosen size m [38, 62].

The lowest excited state $|\psi_1\rangle$ can also be targeted with DMRG [53] provided that $|\psi_0\rangle$ has been pre-calculated. The only difference from a ground-state DMRG algorithm is that one has to maintain the orthogonality condition $\langle\psi_1|\psi_0\rangle = 0$ at each step. Upon reformulating the Hamiltonian for the lowest excited state as $H_1 = H - \lambda_0|\psi_0\rangle\langle\psi_0|$, where λ_0 is the eigenvalue of H corresponding to $|\psi_0\rangle$, one can write down the effective Hamiltonian equation in the DMRG procedure as

$$\left[U_1^\dagger \left(H - \lambda_0|\psi_0\rangle\langle\psi_0|\right) U_1\right] U_1^\dagger|\psi_1\rangle = \lambda_1 U_1^\dagger|\psi_1\rangle, \qquad (1)$$

where U_1 projects onto the canonical MPS [38] for $|\psi_1\rangle$ without the center two sites, as illustrated in Fig. 1, and λ_1 is the eigenvalue for $|\psi_1\rangle$. We can therefore define an effective Hamiltonian $H^1_{\rm eff} \equiv U_1^\dagger \left(H - \lambda_0|\psi_0\rangle\langle\psi_0|\right) U_1$.

Similarly, given that $|\psi_i\rangle$ for all $i < j$ ($\lambda_i < \lambda_j$) have been pre-calculated, we observe that one can compute the next eigenstate j as an MPS with a given number of

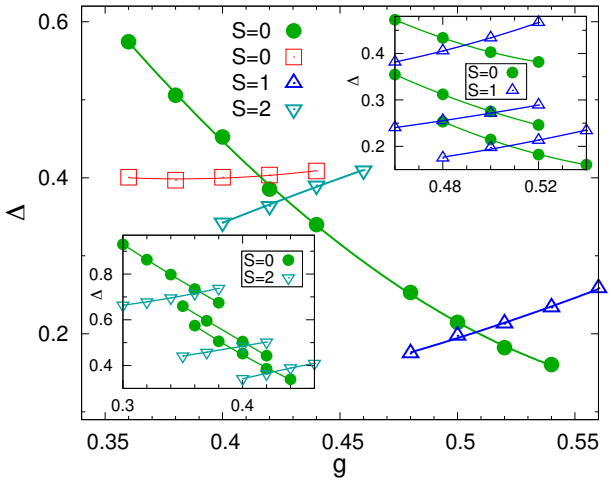

FIG. 2. Gaps to the relevant $S = 0, 1$, and 2 excitations vs g for $L = 10$. The insets show the regions of the level crossings of interest for $L = 6, 8, 10$ (gaps decreasing with increasing L). The curves show polynomial fits.

kept Schmidt states m using a modified Hamiltonian

$$H_j = H - \sum_{i=0}^{j-1} \lambda_i |\psi_i\rangle\langle\psi_i|. \qquad (2)$$

Here $H^j_{\rm eff} U_j^\dagger|\psi_j\rangle = \lambda_j U_j^\dagger|\psi_j\rangle$ as in Eq. (1). In practice such a DMRG scheme will break down (i.e., unreasonably large m has to be used) when the eigenstates far from the bottom of the spectrum begin to violate the area law.

The $2L \times L$ cylinder geometry, with open and periodic boundaries in the x and y direction, respectively, is known to be suitable for 2D DMRG calculations [63] and we use it here for even L up to 10. We employ the DMRG with either U(1) (the total spin z component S^z is conserved) or SU(2) symmetry. With $U(1)$ symmetry, we generate up to ten $S^z = 0$ states and obtain the total spin S by computing the expectation value of $\mathbf{S}^2$.

An advantage of focusing on the level spectrum is the well known fact that the energy converges much faster with the number m of Schmidt states than other physical observables, and also as a function of the number of sweeps in the DMRG procedure. We here apply very stringent convergence criteria and also extrapolate away the remaining finite-m errors based on calculations for several values of m up to $m = 12000$ with $U(1)$ symmetry and $m = 5000$ with $SU(2)$ symmetry. The DMRG procedures and extrapolations are further discussed in Supplemental Material (SM) [64].

Results.—Figure 2 shows two singlet gaps and the lowest triplet and quintuplet gaps versus g in and close to the non-magnetic regime. The main graph shows results for $L = 10$. One of the singlet gaps decreases rapidly with increasing g, crossing the other three levels. This is the lowest singlet excitation starting from $g \approx 0.42$,

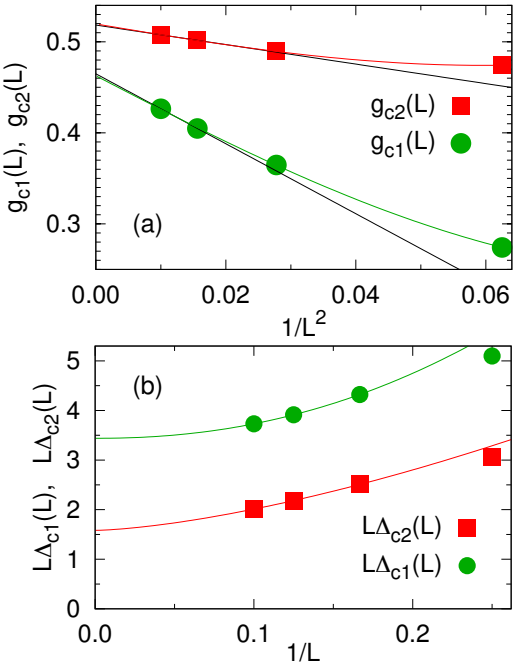

FIG. 3. (a) The gap-crossing points from Fig. 2 graphed vs L^{-2}. For the singlet-triplet (red squares) and singlet-quintuplet (green circles) data sets, the black lines go through the $L = 8, 10$ points, while the colored curves are of the form $g_c(L) = g_c(\infty) + aL^{-2}(1 + bL^{-\omega})$ with $g_{c2}(\infty) \approx 0.519$, $g_{c1}(\infty) \approx 0.463$, and $\omega \approx 4$. (b) Size-scaled gaps at the singlet-quintuplet (Δ_{c1}) and singlet-triplet (Δ_{c2}) crossing points along with fits of the form $L\Delta(L) = c + dL^{-\sigma}$, where $\sigma_1 \approx 2$ and $\sigma_2 \approx 1.5$.

after crossing the other singlet (which has other quantum numbers related to the lattice symmetries) that is lower in what we will argue is the AFM phase. The insets of Fig. 2 show results also for $L = 6$ and 8 in the region around the level crossings that we will analyze (the higher gaps for $L = 4$ are not shown for clarity). Using polynomial fits to the DMRG data points, we extract crossing points $g_{c1}(L)$ between the singlet and the quintuplet, as well as $g_{c2}(L)$ between the singlet and the triplet. The singlet-singlet crossings taking place close to $g_{c1}(L)$ are discussed in the SM [64]; their size dependence is similar to $g_{c1}(L)$. For $g \gtrsim g_{c1}(L)$ there are also other levels in the energy range of Fig. 2, including singlets, but the $S = 0, 1, 2$ gaps graphed are the lowest with these spins up to and beyond the largest g shown.

As L increases the two sets of crossing points drift toward two different asymptotic values. For the singlet-triplet crossings, we have considered different extrapolation procedures with $g_{c2}(L)$, all of which deliver $g_{c2} \approx 0.52$ when $L \to \infty$. It is natural to test whether the finite-size correction to g_{c2} is consistent with the L^{-2} drift in the frustrated Heisenberg chain [54–56]; a behavior also found in the 2D J-Q model in Ref. 59. In Fig. 3(a) we graph the data versus L^{-2} along with a line drawn through the $L = 8$ and $L = 10$ points, as well as a fitted curve including a higher-order correction. Although we have only four points and there are three free parameters, it is not guaranteed that the fit should match the data as well as it does. With a leading L^{-1} correction the best fit is far from good. Therefore, we take the former fit as evidence that the asymptotic drift is at least very close to L^{-2}. The fit with the subleading correction in Fig. 3(a) gives $g_{c2} = 0.519$; a minute change from the straight-line extrapolation. Based on the differences between the two extrapolations and roughly estimated errors on the individual crossing points (which arise from the DMRG extrapolations, as discussed in SM [64]), the final result is $g_{c2} = 0.519 \pm 0.002$.

Plotting the singlet-quintuplet crossing points in the same graph in Fig. 3(a), the overall behavior is similar to the singlet-triplet points, but it is clear that they do not drift as far as to g_{c2}. We find that the L^{-2} form applies also here; see the SM [64] for further analysis of the corrections for both g_{c1} and g_{c2}. A rough extrapolation by a line drawn through the $L = 8$ and $L = 10$ points gives $g_{c1} \approx 0.465$, and when including a correction, of the same form as in the singlet-triplet case, the extrapolated value moves only slightly down to $g_{c1} \approx 0.463$. Based on this analysis we conclude that $g_{c1} = 0.463 \pm 0.002$.

In Fig. 3(b) we analyze the crossing gaps, multiplied by L in order to make clearly visible the leading behavior and well-behaved corrections. All gaps close as L^{-1}, i.e., the dynamic exponent $z = 1$ at both critical points. We have also analyzed the gaps in the regime $g_{c1} < g < g_{c2}$ (not shown), and it appears that the lowest $S = 0, 1, 2$ gaps all scale as L^{-1} throughout. This phase should therefore be a gapless (algebraic) SL, instead of a Z_2 SL with nonzero triplet gap for $L \to \infty$ [28] and singlet gap vanishing exponentially (due to topological degeneracy).

The point $g_{c2} \approx 0.52$ is higher than almost all previous results reported for the point beyond which the AFM order vanishes, but it is close to where recent works have suggested a transition from a gapless SL into a VBS [29, 39]. If there indeed is a gapless SL intervening between the AFM and the VBS phases and its lowest excitation is a triplet (as is the case, e.g., in the critical Heisenberg chain), then a singlet-triplet crossing is indeed expected at the SL–VBS transition, since the triplet is gapped and the ground state is degenerate in the VBS phase.

To interpret the singlet-quintuplet crossing at $g_{c1} \approx 0.46$, we again note that the nature of the low-lying gapless excitations reflect the properties of the ground state, and a ground state transition can be accompanied by rearrangements of levels across sectors or within a sector of fixed total spin. A singlet-quintuplet crossing is indeed present at the transition between a critical Heisenberg state (an 1D algebraic SL) and a long-range AFM state in a spin chain with long-range unfrustrated interactions and either unfrustrated [65] or frustrated [56, 60] short-range interactions, as we discuss further in the SM

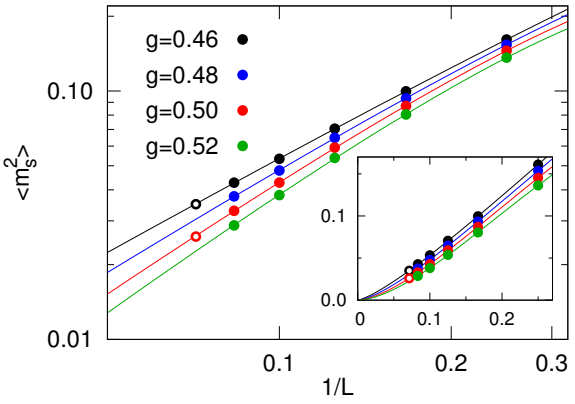

FIG. 4. Log-log plot of $\langle m_s^2 \rangle$ vs L^{-1}. The curves are of the form $\langle m_s^2 \rangle = bL^{-\alpha}(1 - cL^{-\omega})$ with $\omega = 0.5$. The leading exponent, with errors estimated by changing ω within its range of good fits, are $\alpha = 1.35 \pm 0.05$ ($g = 0.46$), 1.53 ± 0.08 ($g = 0.48$), 1.69 ± 0.10 ($g = 0.50$), and 1.78 ± 0.12 ($g = 0.52$). The inset shows the same data on a linear scale. The $L = 14$ data (open circles) are from Ref. 29.

[64]. This analogy, and the fact that g_{c1} is close to where many previous works have located the end of the AFM phase (as we also show below and in SM [64]), provides compelling evidence for the association of the singlet-quintuplet crossing with the AFM–SL transition. Furthermore, the $S = 2$ quantum rotor state in the AFM state has gap $\propto L^{-2}$, while at g_{c1} it scales as L^{-1} according to Fig. 3. Thus, at this point (and for higher g) the level spectrum is incompatible with AFM order.

We also computed the squared AFM order parameter (sublattice magnetization per spin) $\langle m_s^2 \rangle$ in the putative SL phase, with $\mathbf{m}_s$ defined on the central $L \times L$ part of the $2L \times L$ system (here with L up to 12). Since we mainly focused on the excited energies, we did not push the ground state $\langle m_s^2 \rangle$ calculations to as large L as in some past works [28, 29]. To complement our own data, we therefore also use $L = 14$ results from Ref. 29. In cases where we have data for the same parameter values, our results agree to within 0.2%. We fit the data to power laws with a correction; $\langle m_s^2 \rangle = bL^{-\alpha}(1 - cL^{-\omega})$, where acceptable values of ω span the range $\omega \approx 0.2 \sim 1.5$ and the exponent α changes somewhat when varying ω. In Fig. 4 we show examples of fits with $\omega = 0.5$. We find that α increases with g, from $\alpha \approx 1.3$ at $g = 0.46$ to $\alpha \approx 1.8$ at $g = 0.52$. We have also tried to fix α to a common value for all g, but this does not produce good fits. We therefore agree with previous claims [29, 39] that the exponent depends on g. At $g = 0.5$, our result $\alpha \approx 1.7 \pm 0.1$ is larger than the value 1.44 reported in Ref. 29, with the difference explained by the correction used here. The result agrees well with $\alpha = 1.53 \pm 0.09$ from variational Monte Carlo calculations [39], and a similar value was also reported with a projected entangled pair state ansatz [21]. In the SM [64] we provide further analysis showing that the AFM order vanishes at the extrapolated level crossing point $g_{c1} \approx 0.46$.

Discussion.—Our level-crossing analysis in combination with results for the sublattice magnetization show consistently that the AFM phase ends at $g_{c1} \approx 0.46$ and a gapless SL phase exists between this value and $g_{c2} \approx 0.52$. In the level crossing approach the finite-size transition points are sharply defined and the convergence with system size is rapid, with corrections vanishing as L^{-2} (or possibly L^{-a} with $a \approx 2$). Our results in Fig. 3(a) leave little doubt that the singlet-quintuplet and singlet-triplet crossings converge to different points, while we would expect convergence to the same point if there is no SL between the AFM and VBS phases, as we demonstrate explicitly in the SM [64] in the case of the J-Q model. The behavior of the spin correlations and the gaps imply a gapless SL with power-law decaying spin correlations. In the region $0.52 < g < 0.62$, between the SL and the stripe-AFM, our calculations of excited states reveal many low-lying singlets, and we have been able to map them [66] onto the expected quasi-degenerate levels expected for a columnar [39] VBS state.

The AFM–SL and SL–VBS phase boundaries are in rough agreement with two recent works discussing a gapless SL phase followed by a VBS [29, 39], and the lower boundary agrees well with a Lanczos-improved variational Monte Carlo calculation [27]. Many other past studies have located the end of the AFM order close to the same value. A recent exception is an infinite-size tensor calculation [33] where the AFM order ends close to our g_{c2} point. However, the infinite-size approach is not unbiased but depends on details of how the environment tensors are constructed. The DMRG calculations, here and in Ref. 29, are unbiased for finite size if the convergence is checked carefully, and completely exclude AFM order beyond our g_{c1} value.

As far as we are aware, the critical singlet-quintuplet crossing found here (and the singlet-singlet crossing in the SM [64]) has not previously been discussed in the 2D context. This level crossing has been considered in 1D [56, 60], and in the SM [64] we present additional evidence of its association with the AFM–SL transition. The physical origin of the level crossing deserves further study. The detailed information we have obtained on the evolution of the low-energy levels in 2D should be useful for discriminating between different field theoretical descriptions of the phase transitions and the SL phase.

We expect that level crossings are common at 2D quantum phase transitions, as they are in 1D. Our work suggests that the best way to use 2D DMRG in studies of quantum criticality is to first look for and analyze level crossings to extract critical points, and then study order parameters (conventional or topological) at this point and in the phases. In principle the DMRG procedures that we have employed here can also be extended to more detailed level-spectroscopy studies [59, 67].

Acknowledgments.—We would like to thank F. Becca, S. Capponi, M. Imada, D. Poilblanc, S. Sachdev, J.-Z. Zhao, and Z.-Y. Zhu, for helpful discussions. We are grateful to S. Gong and D. Sheng for providing their numerical results from Ref. 29. L.W. is supported by the National Key Research and Development program of China (Grant No. 2016YFA0300600), the National Natural Science Foundation of China (Grant No. NSFC-11734002 and No. NSFC-11474016), the National Thousand Young Talents Program of China, and the NSAF Program of China (Grant No. U1530401). She thanks Boston University's Condensed Matter Theory Visitors program for travel support. A.W.S. was supported by the NSF under grants No. DMR-1410126 and DMR-1710170, and by a Simons Investigator Grant. He would also like to thank the Beijing Computational Science Research Center (CSRC) for visitor support. The calculations were partially carried out under a Tianhe-2JK computing award at the CSRC.

* lingwang@csrc.ac.cn
† sandvik@bu.edu

[1] P. Chandra and B. Doucot, Possible spin-liquid state at large S for the frustrated square Heisenberg lattice, Phys. Rev. B **38**, 9335 (1988).
[2] E. Dagotto and A. Moreo, Phase diagram of the frustrated spin-1/2 Heisenberg antiferromagnet in 2 dimensions, Phys. Rev. Lett. **63**, 2148 (1989).
[3] M. P. Gelfand, R. R. P. Singh, and D. A. Huse, Zero-temperature ordering in two-dimensional frustrated quantum Heisenberg antiferromagnets, Phys. Rev. B **40**, 10801 (1989).
[4] S. Sachdev, Large-N limit of the square-lattice t-J model at 1/4 and other filling fractions, Phys. Rev. B **41**, 4502 (1990).
[5] F. Figueirido, A. Karlhede, S. Kivelson, S. Sondhi, M. Rocek, and D. S. Rokhsar, Exact diagonalization of finite frustrated spin-1/2 Heisenberg models, Phys. Rev. B **41**, 4619 (1990).
[6] R. R. P. Singh and R. Narayanan, Dimer versus twist order in the J_1-J_2 model, Phys. Rev. Lett. **65**, 1072 (1990).
[7] N. Read and S. Sachdev, Large-N expansion for frustrated quantum antiferromagnets, Phys. Rev. Lett. **66**, 1773 (1991).
[8] H. J. Schulz and T. A. L. Ziman, Finite-Size Scaling for the Two-Dimensional Frustrated Quantum Heisenberg Antiferromagnet, Europhys. Lett. **18**, 355 (1992).
[9] N. E. Ivanov and P. Ch. Ivanov, Frustrated two-dimensional quantum Heisenberg antiferromagnet at low temperatures, Phys. Rev. B **46**, 8206 (1992).
[10] T. Einarsson and H. J. Schulz, Direct calculation of the spin stiffness in the J_1-J_2 Heisenberg antiferromagnet, Phys. Rev. B **51**, 6151 (1995).
[11] H. J. Schulz, T. A. L. Ziman, and D. Poilblanc, Magnetic Order and Disorder in the Frustrated Quantum Heisenberg Antiferromagnet in Two Dimensions, J. Phys. I **6**, 675 (1996).
[12] R. R. P. Singh, Z. Weihong, C. J. Hamer, and J. Oitmaa, Dimer order with striped correlations in the J_1-J_2 Heisenberg model, Phys. Rev. B **60**, 7278 (1999).
[13] P. Fazekas and P. W. Anderson, On the ground state properties of the anisotropic triangular antiferromagnet, Philos. Mag. **30**, 432 (1974).
[14] P. W. Anderson The resonating valence bond state in La_2CuO_4 and superconductivity, Science **235**, 1196 (1987).
[15] For a review, see P. A. Lee, N. Nagaosa, and X. G. Wen, Doping a Mott insulator: Physics of high-temperature superconductivity, Rev. Mod. Phys. **78**, 17 (2006).
[16] H. T. Diep, Editor, *Frustrated Spin Systems* (World Scientific, 2005).
[17] L. Capriotti and S. Sorella, Spontaneous Plaquette Dimerization in the J_1-J_2 Heisenberg Model, Phys. Rev. Lett. **84**, 3173 (2000).
[18] J. Sirker, Z. Weihong, O. P. Sushkov, and J. Oitmaa, J_1-J_2 model: First-order phase transition versus deconfinement of spinons, Phys. Rev. B **73**, 184420 (2006).
[19] R. Darradi, O. Derzhko, R. Zinke, J. Schulenburg, S. E. Krüger, and J. Richter, Ground state phases of the spin-1/2 J_1-J_2 Heisenberg antiferromagnet on the square lattice: A high-order coupled cluster treatment, Phys. Rev. B **78**, 214415 (2008).
[20] L. Wang, Z.-C. Gu, F. Verstraete, and X.-G. Wen, Tensor-product state approach to spin-1/2 square J_1-J_2 antiferromagnetic Heisenberg model: Evidence for deconfined quantum criticality, Phys. Rev. B **94**, 075143 (2016).
[21] D. Poilblanc and M. Mambrini, Quantum critical point with infinite projected entangled paired states, Phys. Rev. B **96**, 014414 (2017).
[22] L. Capriotti, F. Becca, A. Parola, and S. Sorella, Resonating Valence Bond Wave Functions for Strongly Frustrated Spin Systems, Phys. Rev. Lett. **87**, 097201 (2001).
[23] M. Mambrini, A. Läuchli, D. Poilblanc, and F. Mila, Plaquette valence-bond crystal in the frustrated Heisenberg quantum antiferromagnet on the square lattice, Phys. Rev. B **74**, 144422 (2006).
[24] M. Arlego and W. Brenig, Plaquette order in the J_1-J_2-J_3 model: Series expansion analysis, Phys. Rev. B **78**, 224415 (2008).
[25] K. S. D. Beach, Master equation approach to computing RVB bond amplitudes, Phys. Rev. B **79**, 224431 (2009).
[26] J. Richter and J. Schulenburg, The spin-1/2 J_1-J_2 Heisenberg antiferromagnet on the square lattice: Exact diagonalization for $N = 40$ spins, Eur. Phys. J. B **73**, 117 (2010).
[27] W.-J. Hu, F. Becca, A. Parola, and S. Sorella, Direct evidence for a gapless Z_2 spin liquid by frustrating Néel antiferromagnetism, Phys. Rev. B **88**, 060402(R) (2013).
[28] H.-C. Jiang, H. Yao, and L. Balents, Spin Liquid Ground State of the Spin-1/2 Square J_1-J_2 Heisenberg Model, Phys. Rev. B **86**, 024424 (2012).
[29] S.-S. Gong, W. Zhu, D. N. Sheng, O. I. Motrunich, and M. P. A. Fisher, Plaquette Ordered Phase and Quantum Phase Diagram in the Spin-1/2 J_1-J_2 Square Heisenberg Model, Phys. Rev. Lett. **113**, 027201 (2014).
[30] V. Murg, F. Verstraete, and J. I. Cirac, Exploring frustrated spin systems using projected entangled pair states, Phys. Rev. B **79**, 195119 (2009).
[31] J. F. Yu and Y. J. Kao, Spin-1/2 J_1-J_2 Heisenberg antiferromagnet on a square lattice: a plaquette renormalized tensor network study, Phys. Rev. B **85**, 094407 (2012).

[32] L. Wang, D. Poilblanc, Z.-C. Gu, X.-G. Wen, and F. Verstraete, Constructing gapless spin liquid state for the spin-1/2 J_1-J_2 Heisenberg model on a square lattice, Phys. Rev. Lett. **111**, 037202 (2013).

[33] R. Haghshenas, D. N. Sheng, U(1)-symmetric infinite projected entangled-pair state study of the spin-1/2 square J_1J_2 Heisenberg model, Phys. Rev. B **97**, 174408 (2018).

[34] P. W. Anderson, An Approximate Quantum Theory of the Antiferromagnetic Ground State, Phys. Rev. **86**, 694 (1952).

[35] S. Chakravarty, B. I. Halperin, and D. R. Nelson, Two-dimensional quantum Heisenberg antiferromagnet at low temperatures, Phys. Rev. B **39**, 2344 (1989).

[36] E. Manousakis, The spin-1/2 Heisenberg antiferromagnet on a square lattice and its application to the cuprous oxides, Rev. Mod. Phys. **63**, 1 (1991).

[37] S. R. White, Density matrix formulation for quantum renormalization groups, Phys. Rev. Lett. **69**, 2863 (1992).

[38] U. Schollwöck, The density-matrix renormalization group in the age of matrix product states, Ann. Phys. **326**, 96 (2011).

[39] S. Morita, R. Kaneko, and M. Imada, Quantum Spin Liquid in Spin 1/2 J_1J_2 Heisenberg Model on Square Lattice: Many-Variable Variational Monte Carlo Study Combined with Quantum-Number Projections, J. Phys. Soc. Jpn. **84**, 024720 (2015).

[40] T. Senthil, A. Vishwanath, L. Balents, S. Sachdev, and M. Fisher, Deconfined quantum critical points, Science **303**, 1490 (2004).

[41] T. Senthil, L. Balents, S. Sachdev, A. Vishwanath, and M. P. A. Fisher, Quantum criticality beyond the Landau-Ginzburg-Wilson paradigm, Phys. Rev. B **70**, 144407 (2004).

[42] E. G. Moon and C. Xu, Exotic continuous quantum phase transition between Z_2 topological spin liquid and Néel order, Phys. Rev. B **86**, 214414 (2012).

[43] A. W. Sandvik, Evidence for Deconfined Quantum Criticality in a Two-Dimensional Heisenberg Model with Four-Spin Interactions, Phys. Rev. Lett. **98**, 227202 (2007).

[44] R. G. Melko and R. K. Kaul, Scaling in the Fan of an Unconventional Quantum Critical Point, Phys. Rev. Lett. **100**, 017203 (2008).

[45] J. Lou, A. W. Sandvik, and N. Kawashima, Antiferromagnetic to valence-bond-solid transitions in two-dimensional $SU(N)$ Heisenberg models with multispin interactions, Phys. Rev. B **80**, 180414(R) (2009).

[46] A. Banerjee, K. Damle, and F. Alet, Impurity spin texture at a deconfined quantum critical point, Phys. Rev. B **82**, 155139 (2010).

[47] M. S. Block, R. G. Melko,and R. K. Kaul, Fate of CP^{N-1} Fixed Points with q Monopoles, Phys. Rev. Lett. **111**, 137202 (2013).

[48] K. Harada, T. Suzuki, T. Okubo, H. Matsuo, J. Lou, H. Watanabe, S. Todo,and N. Kawashima, Possibility of deconfined criticality in $SU(N)$ Heisenberg models at small N, Phys. Rev. B **88**, 220408 (2013).

[49] K. Chen, Y. Huang, Y. Deng, A. B. Kuklov, N. V. Prokofev,and B. V. Svistunov, Deconfined Criticality Flow in the Heisenberg Model with Ring-Exchange Interactions, Phys. Rev. Lett. **110**, 185701 (2013).

[50] H. Shao, W. Guo, and A. W. Sandvik, Quantum criticality with two length scales, Science **352**, 213 (2016).

[51] A. Nahum, J. T. Chalker, P. Serna, M. Ortuño,and, A. M. Somoza, Deconfined Quantum Criticality, Scaling Violations, and Classical Loop Models, Phys. Rev. X **5**, 041048 (2015).

[52] E. M. Stoudenmire and S. R. White, Real-space parallel density matrix renormalization group, Phys. Rev. B **87**, 155137 (2013).

[53] I. P. McCulloch, From density-matrix renormalization group to matrix product states, J. Stat. Mech. **2007**, P10014 (2007).

[54] K. Nomura and K. Okamoto, Spin-Gap Phase in the One-Dimensional t-J-J' Model, Phys. Lett. A **169**, 433 (1992).

[55] S. Eggert, Numerical evidence for multiplicative logarithmic corrections from marginal operators, Phys. Rev. B **54**, R9612 (1996).

[56] A. W. Sandvik, Ground States of a Frustrated Quantum Spin Chain with Long-Range Interactions, Phys. Rev. Lett. **104**, 137204 (2010).

[57] A. W. Sandvik, Computational Studies of Quantum Spin Systems, AIP Conf. Proc. **1297**, 135 (2010).

[58] H. Suwa and S. Todo, Generalized Moment Method for Gap Estimation and Quantum Monte Carlo Level Spectroscopy, Phys. Rev. Lett. **115**, 080601 (2015).

[59] H. Suwa, A. Sen, and A. W. Sandvik, Level spectroscopy in a two-dimensional quantum magnet: Linearly dispersing spinons at the deconfined quantum critical point, Phys. Rev. B **94**, 144416 (2016).

[60] In Ref. [56], the crossing $S = 2$ state was misidentified as a singlet, but the results otherwise agree with our DMRG calculations presented in Supplemental Material [64].

[61] A. W. Sandvik, Finite-size scaling and boundary effects in two-dimensional valence-bond solids, Phys. Rev. B **85**, 134407 (2012)

[62] S. Östlund and S. Rommer, Thermodynamic Limit of Density Matrix Renormalization, Phys. Rev. Lett. **75**, 3537 (1995).

[63] S. R. White and A. L. Chernyshev, Néel Order in Square and Triangular Lattice Heisenberg Models, Phys. Rev. Lett. **99**, 127004 (2007).

[64] See Supplemental Material for discussion of the convergence of the DMRG calculations, level crossings in the the 2D J-Q model and the 1D model with long-range interactions, additional analysis of the AFM order of the 2D J_1-J_2 model, as well as the level crossings of its two lowest singlet excitations.

[65] N. Laflorencie, I. Affleck, and M. Berciu, J. Stat. Mech. (2005) P12001.

[66] L. Wang, S. Capponi, H. Shao, and A. M. Sandvik, (unpublished)

[67] M. Schuler, S. Whitsitt, L. P. Henry, S. Sachdev, and A. M. Läuchli, Universal Signatures of Quantum Critical Points from Finite-Size Torus Spectra: A Window into the Operator Content of Higher-Dimensional Conformal Field Theories, Phys. Rev. Lett. **117**, 210401 (2016).